Available online at www.sciencedirect.com
ScienceDirect
Journal of Nuclear Materials 363–365 (2007) 382–388
journal of nuclear materials
www.elsevier.com/locate/jnucmat

Sheath heat transmission factors on TCV

J. Marki [a,*], R.A. Pitts [a], T. Eich [b], A. Herrmann [b], J. Horacek [a], F. Sanchez [a], G. Veres [c]

[a] *Centre de Recherches en Physique des Plasmas, Association EURATOM-Confédération Suisse, École Polytechnique Fédérale de Lausanne, CH-1015, Switzerland*
[b] *Max-Planck-Institut für Plasmaphysik, EURATOM Association, D-85740 Garching, Germany*
[c] *RMKI-KFKI, HAS EURATOM, H-1121 Budapest, Hungary*

Abstract

Despite its importance in determining the calculated surface power flux predicted, for example, by scrape-off layer simulation codes, the sheath heat transmission factor, γ remains a quantity whose theoretically predicted value has rarely been tested experimentally. This contribution attempts such a test by comparing direct, infra-red measurements of the outer divertor target power fluxes in single null lower discharges on the TCV tokamak with tile embedded Langmuir probe data. A selection of L-mode plasmas have been used, including varying outer target flux expansion and a pair of matched D–He pulses. Particular care is taken to identify all possible sources of error and estimate their effect on the derived values of γ. Within the admittedly rather large uncertainty, L-mode values of γ are found to be consistent with simple sheath theory.

PACS: 52.25.Rv; 52.40.Hf; 52.55.Dy; 52.70.Kz

Keywords: Divertor plasma; Power deposition; Sheaths; TCV; Thermography

1. Introduction

One of the major challenges for any future fusion power plant is the expected excessive heat load on the divertor targets. Predictions of these heat loads rely largely on fluid-code simulations, in which the heat transfer across the sheath (an inherently kinetic process) is computed using analytic expressions derived from simple sheath theory. The heat transfer is characterized by the total sheath heat transmission coefficient γ, for which in the far from ideal situation of the tokamak divertor (glancing magnetic field line angles, non-smooth surfaces, often with unknown surface composition, etc.), the existing dataset is far from being sufficient to verify the validity of the analytic theory.

A number of attempts on a variety of tokamaks have been reported in the literature to derive steady state (as opposed to time varying values during transient events such as ELMs) experimental values of γ. The results are compiled in Table 1. This paper adds a further contribution to this database by presenting some results from the first attempt to measure γ on the TCV tokamak. Measurements have

* Corresponding author.
E-mail address: janos.marki@epfl.ch (J. Marki).

0022-3115/$ - see front matter
doi:10.1016/j.jnucmat.2007.01.197

Table 1
Compilation of reported data for the measurement of total sheath heat transmission factors in tokamaks

Tokamak	Range of γ	Refs.
ASDEX-Upgrade	3–8	[1]
DIII-D	2–4	[2]
JET	2–8	[3]
JT-60U	2–20	[4]
TEXT	~5	[5]
Tore Supra	2–11	[6]
TCV	4–8	This paper

been performed using a combination of IR thermography and divertor target embedded Langmuir probes where, crucially, the probes are located entirely within the IR camera field of view.

Working mostly in low density L-mode discharges (to avoid detachment of the divertor plasma), provides the simplest possible conditions, but even here, the cumulative effect of a number of key uncertainties leads to a rather large error bar on the derived values of the sheath heat transmission coefficient. Nevertheless, we will show that the theoretically expected values are, within errors, retrieved experimentally, at least under simple, non-transient conditions.

2. Theoretical background

An electrostatic sheath will form at any plasma boundary and acts to filter all but the high energy electrons whilst attracting ions, controlling the energy flux leaving the plasma. Each ion–electron pair crossing the sheath convects to the surface a quantity of energy which is conventionally described using a total sheath heat transmission coefficient where [7]

$$q_{se} = \gamma \cdot kT_e \cdot \Gamma_{se} \tag{1}$$

with q_{se} total heat flux at the sheath edge, T_e the electron temperature, Γ_{se} the sheath edge particle flux and where

$$\gamma = 2.5\frac{T_i}{T_e} + \frac{2}{1-\delta_e} - 0.5\ln\left[\left(2\pi\frac{m_e}{m_i}\right)\left(1+\frac{T_i}{T_e}\right)\frac{2}{(1-\delta_e)^2}\right] \tag{2}$$

with δ_e the electron secondary electron emission (s.e.e.) coefficient and T_i the ion temperature. To estimate γ using (2) requires knowledge of T_i and δ_e, but both are usually inaccessible at the divertor targets. An alternative is to use direct measurements of the surface heat flux and compare with the values inferred from Langmuir probes (LP) which in fact measure the current–voltage characteristic of the sheath itself

$$p_{LP} = \gamma \cdot kT_e \cdot \Gamma_{se}\sin\vartheta = \gamma \cdot kT_e \cdot \frac{j_{sat}}{e} \cdot \sin\vartheta = P_{IR}, \tag{3}$$

where P_{LP} and P_{IR} are respectively the Langmuir probe and IR inferred heat fluxes, ϑ is the impact angle between the total magnetic field and the target surface and j_{sat} is the measured ion saturation current density. In estimating the γ in (2), a number of additional contributing factors can in principle be included, such as pre-sheath acceleration, ion–electron surface recombination energy, particle reflection and secondary electron emission (both ion and electron induced, to be abbreviated by s.e.e.), however, all of these are problematic:

- The pre-sheath contribution to is $\gamma_{ps} \sim 0.5$, but this can vary in case of a complex pre-sheath [7].
- The contribution of ion–electron surface recombination energy, taking into account the energy needed to release an electron from the surface (the work function) and the energy released by atom–atom recombination to molecules is $\gamma_{rec} \sim 0.3$. As demonstrated in Section 4.2.2, the TCV divertor plates are covered by layers of unknown composition, and thus the exact value of the work function cannot be known, rendering a precise determination of this term impossible.
- Secondary electrons may be emitted both due to incoming ions and electrons, for both of which cases there exist laboratory measurements indicating the respective s.e.e. coefficients δ_{ee} and δ_{ie}. These are, however, performed with monoenergetic beams on pure material surfaces and are not applicable to layers of unknown composition with Maxwellian incident particle distributions.
- Particle reflection (electron- as well as ion reflection), even though data exists in the scientific literature, is also target-specific, so because of the surface layers, an exact value cannot be determined for it.

As a last measure to obtain an estimate for γ, we assume $T_i = T_e$. This assumption has been verified by previous SOLPS5 code simulations for the plasma conditions used here [8].

To compare our experimental results with the theory described here, we will use a simplified approach by neglecting all of the above problematic terms, leading to $\gamma = 7$ from Eq. (2). In order to see the effect of the neglected terms, we are making an estimate of γ using the best possible values for all of the cited terms. We assume an isothermal fluid estimate for the pre-sheath potential ($\sim 0.7\, kT_e$ [7]), the work function for clean graphite $W = 4.6$ eV, a total secondary electron emission coefficient $\delta_e = 0.5$ and the following reflection coefficients: $R_{Ni} = 0.25$, $R_{Ne} = 0.08$, $R_{Ei} = 0.1$, $R_{Ee} = 0.08$ for the ion and electron number and energy reflection coefficients, respectively. The electron s.e.e. is estimated using the known two-parameter semi-empiric formula with the parameters taken from electron beam measurements performed on pyrolytic graphite surfaces previously exposed to various plasma environments [9] whilst the ion s.e.e. is derived from real-time, in-situ measurements reported from DITE [10]. The ion reflection coefficients have been taken from reported data on deuterium bombardment of clean graphite [11], and the electron reflection from electron bombardment of clean graphite [12]. Adding these terms yields $\gamma = 8.8$, 20% higher than the simple value. As we shall see later, this difference is well within the experimental error bars, justifying the neglect of the extra terms in Eq. (2).

3. Experiment

Following the approach in [13], we combine IR thermography of the TCV outer target in combination with tile embedded Langmuir probes to measure P_{IR} and P_{LP} in (2) and hence derive an experimental value for γ. In addition, thermometry using thermocouples installed in the divertor target has been used to cross-check the IR measured power (see Section 4.3). Crucially, as illustrated in Fig. 1, all diagnostics used here are located in the same toroidal sector, such that the Langmuir probes and thermocouples are within the IR field of view. This eliminates toroidal asymmetries as one source of uncertainty in the determination of γ [14].

Fine grained, polycrystalline graphite armour tiles protect the TCV vacuum vessel wall to ~90% of the surface area [15]. In particular, the outer target tiles are machined from the graphite type FP 379 supplied by Schunk.

To measure P_{LP}, an array of domed, graphite single Langmuir probes [16] are voltage scanned at

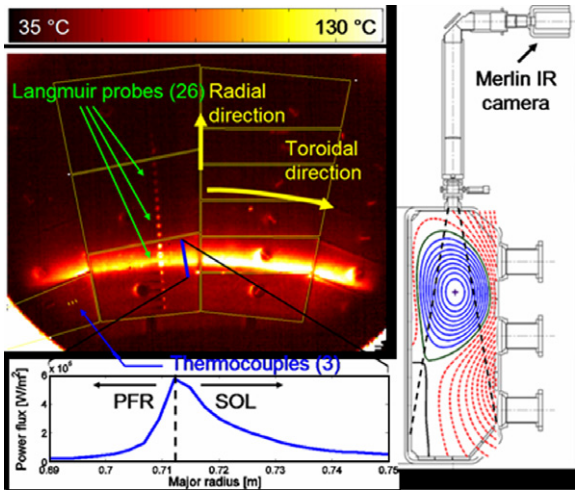

Fig. 1. Illustrating the disposition of divertor diagnostics used in this paper: the 2D surface temperature distribution (shown on the left for TCV shot #29981) is measured by an LWIR microbolometer IR camera viewing the outer divertor target. A typical derived IR power profile is shown on the lower left. The array of tile embedded single Langmuir probes as well as the arc of the strike point zone are clearly visible in the IR image.

100 Hz to provide profiles of T_e and j_{sat}. Two dimensional surface temperature measurements are obtained with an IR camera viewing the vessel floor. The device is of the new uncooled microbolometer generation, operating at 50 Hz in the LWIR range (7–14 μm) and equipped with a 320×240 pixel focal plane array (FPA) with 51 μm pixel pitch. Germanium relay optics project an image of the vessel floor (see Fig. 1) onto the FPA through a ZnSe vacuum window. To compute P_{IR} in (3) from the temperature data, inverse solutions of the heat conduction equation are calculated using the THEODOR code [17] developed at ASDEX-Upgrade but now employed for such analysis on a variety of tokamaks (e.g. JET, MAST).

We have investigated the behaviour of γ in a selected parameter range: L-mode shots with varying field line attack angles and two matched L-mode shots with He and D as bulk species. All plasmas are single null lower (SNL) diverted configurations with ohmic heating only and, in all cases, the discharge density has been maintained low enough to ensure that the outer divertor plasma remains attached. In all these shots, constant density waveforms with line averaged density in the range $\bar{n}_e = 4.5 - 7 \cdot 10^{18}\ m^{-3}$ were used, with plasma currents and ohmic heating power in the range $I_p = 340$–430 kA and $P_{OH} = 375$–475 kW, respectively.

4. Results

4.1. Values of γ

Radial profiles of γ derived according to (3) are shown in the series of Figs. 2–4 for the various experimental conditions described above. To compute radial profiles of P_{IR}, a toroidal band of several pixels on the target tiles housing the Langmuir probes (see Figs. 1 or 4) is averaged at each radius. From this, P_{IR} is calculated by the THEODOR code from the temporal evolution of this toroidally averaged radial profile. The value of γ is then calculated from a steady-state IR power profile averaged over a time window of ~100 ms. Care is taken to choose the surface in question in a zone of uniform power deposition close to the probes but sufficiently distant from tile edges. The error bar associated with each point is obtained from a careful assessment of the various experimental uncertainties that have been considered, each of which is discussed in further detail below.

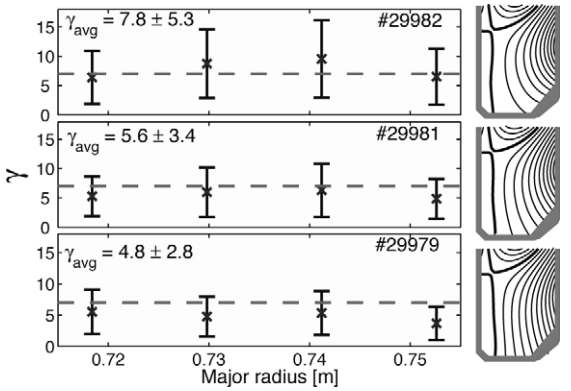

Fig. 2. Profiles of γ across the outer target with increasing divertor flux expansion (and hence decreasing field line attack angle). The horizontal dashed line denotes the expected value of γ (Eq. (2)) for the simplifying assumptions from Section 2. To the right, poloidal cross-sections of the TCV magnetic equilibrium.

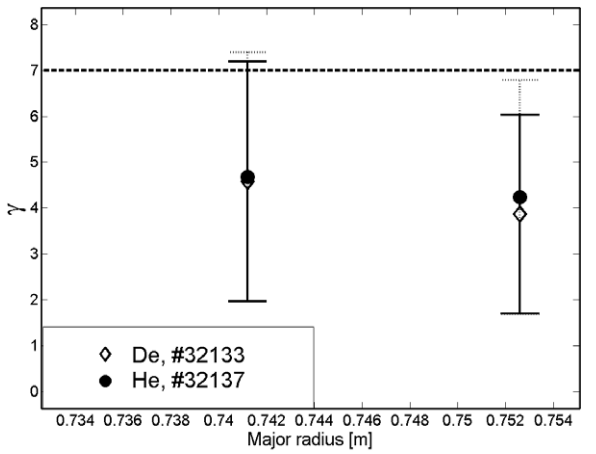

Fig. 3. Profiles of γ across the outer target for matched D and He discharges ($\vartheta = 3°$). The horizontal dashed line denotes the expected value of γ (Eq. (2)) for the simplifying assumptions from Section 2.

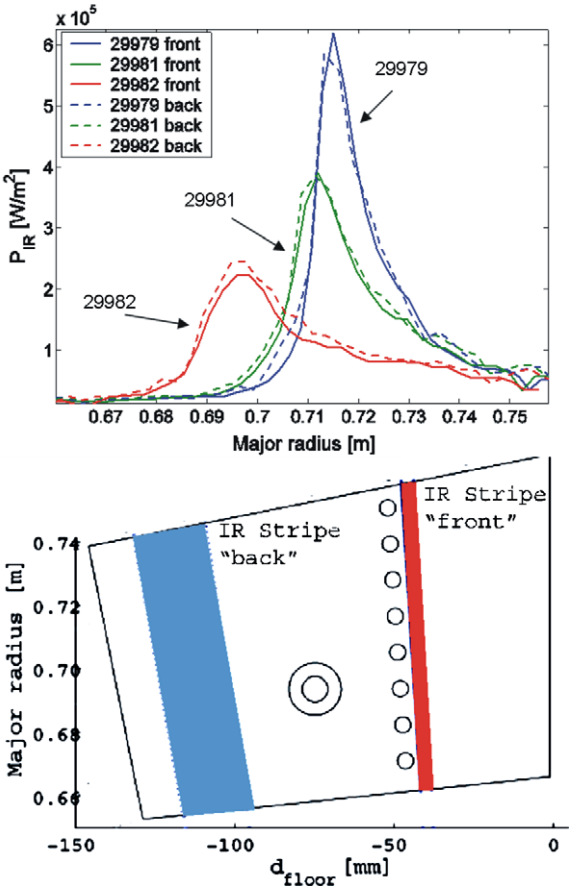

Fig. 4. Comparing toroidally averaged profiles between two radial slices on a tile for different flux expansions. The wider stripe is from the end of the tile where no shadowing can occur and the thinner one from right in front of the LPs (bottom). Profiles from both locations (top) are almost identical for the 3 different attack angles (3°, 1.8° and 1°), therefore it can be concluded that the probes are not shadowed by adjacent tiles.

Fig. 2 investigates the effect of field line attack angle on the derived γ. This is achieved by increasing the outer target flux expansion, f_{exp}, in separate, otherwise identical discharges. As f_{exp} increases, ϑ decreases from 3° to 1° and γ increases from a profile averaged value of 5.2 ± 3.1 for $\vartheta > 1°$ to 7.8 ± 5.3 for $\vartheta = 1°$. Even at these extreme glancing

angles, we do not believe that tile misalignments can be responsible for this behaviour (see below).

Fig. 3 demonstrates that γ is experimentally unchanged for a matched helium and deuterium fueled discharge pair (with $\gamma = 4.4 \pm 2.9$). This is expected theoretically, since for the simplifying assumptions from Section 2, a difference in γ of only 0.2 (due to the ion mass difference) is expected from (2).

4.2. Experimental uncertainties

Unfortunately, both the IR and LP measurements are associated with a number of experimental uncertainties. Each will have an impact on the accuracy of the derived value of γ. Below we discuss explicitly the most important factors, attempting to quantify in each case the expected uncertainty.

4.2.1. Langmuir probe data uncertainties

It is well known that Langmuir probe interpretation in strong magnetic fields and at glancing angles can be problematic [18]. Nevertheless, the probe I–V characteristics for all data used here have been carefully inspected and found to show no signs, for example, of lack of ionic saturation or non-exponential behaviour (below floating potential). The use of low densities (T_e in the divertor is generally $\geqslant 10$ eV for all values of γ computed here) for these experiments also avoids strong recycling regimes known, for a variety of reasons, to lead to overestimates of T_e when using divertor probes [7]. In fact, any such overestimate would decrease the apparent γ (3) and this is in fact partially supported by our L-mode data (Figs. 2 and 3) which generally find γ lower (but not much lower) than expected. Regarding j_{sat}, uncertainty in the probe projected surface area, $A_\perp$, constitutes the most likely source of error, but this is unlikely to be a major factor given that $A_\perp$ for a domed probe changes by $<10\%$ for ϑ in the range 1–3°. Finite ion Larmor effects can be excluded based on the fact that the ion gyroradius for our experimental conditions is small compared to the probe dimensions. Of course, the sin ϑ factor in (3) means that an uncertainty in ϑ itself or a tilt angle of the tile housing the probe are potentially large error sources in the determination of P_{LP}. We are unable to quantify the error in ϑ from the magnetic reconstruction and tilt angles have not yet been measured. The IR 2D surface temperature observations (see Fig. 1), do show some variations in the profile from tile to tile, but there is no evidence from profiles of j_{sat} and P_{IR} as ϑ decreases for any systematic trend for significant tile or probe shadowing (see Section 4.2.2).

To quantify the error on P_{LP}, we thus simply use the statistical average and standard deviation of j_{sat} and T_e over the time intervals used to calculate the value of γ from the IR ($\sim$100 ms). Maximum typical errors are of order 25% estimated in this way.

4.2.2. Infrared data uncertainties

Infrared cameras deduce surface temperatures from the IR radiation emitted by the surface in the camera-specific wavelength band. There are three main problems associated with deducing the total power flux arriving at the divertor: unknown emissivity values, surface layers and tile misalignments.

4.2.2.1. Unknown emissivity values. The emitted thermal radiation as described by the Planck law depends on the surface emissivity ε. Its true value depends on a number of factors (e.g. surface composition and roughness) and is likely to vary with time, possibly even within a single discharge. Considering the fact that we do not have thermocouples in the investigated tile and were thus unable to get an estimate of the emissivity for the signal-temperature conversion, we have worked with $\varepsilon = 1$. For the emissivity range typical for graphite (0.75–0.95), this assumption will introduce a systematic error, which we evaluated by simply using Planck's law. The MERLIN camera integrates in the 7–14 μm range – if the emissivity is lower than assumed, then in reality, a higher temperature will be necessary to yield the same number of photons as those calculated from our $\varepsilon = 1$ assumption, therefore the temperature value deduced will be too low. By looking at the maxima and FWHM of individual profiles, we have estimated the maximum extent of this error for each case considered, which yielded uncertainties of up to 20%.

4.2.2.2. Surface layers. It is well known that in the presence of transient heat fluxes, thin layers deposited on target surfaces respond more quickly than the bulk material and reach much higher temperatures [17]. In the experiments described here, the

transient results both at the beginning and end of the IR measurement when the divertor leg appears and disappears (on a timescale faster than the frame time) in front of the camera. When calculating the heat flux from the spatio-temporal temperature data by assuming a clean graphite surface, an unphysical upward heat flux from the tile surface results after the end of the pulse. Such layers are clearly present in TCV (from multiple boronisations and erosion/redeposition during plasma). To account for this anomalous behaviour, the THEODOR code allows for an adjustable, linear heat transfer term to be introduced into the model. A heat transfer coefficient, α is used, such that the heat flux into the tile is $q = \alpha \times (T_{\mathrm{meas}} - T_{\mathrm{bulk}})$. The layer thickness can be expressed as $d = \kappa_{\mathrm{layer}}/\alpha$ with κ_{layer} the layer thermal conductivity. Care must be taken not to overemphasise the layer thickness – doing so yields unrealistically low heat fluxes. For each discharge studied, α is varied until the negative heat flux experienced at the end of plateau phase of the discharge is eliminated. An example of this procedure is shown in Fig. 5.

For simplicity, we have decided to use a single value of α for the whole profile, but since the layers are far from homogeneous even on a single tile, for different radial locations, different α's were found to be adequate. In some cases, temperature changes due to inter-tile heat mixing (a process occurring usually on a 5 s time-scale) also made it difficult to find the right value of α. These factors led to us having to consider a range of possible α's. The adopted value was the mean of this range and the associated uncertainty was found by looking at the differences in the power fluxes calculated with the mean and the edge values of the α range, which resulted sometimes in values as high as 20%.

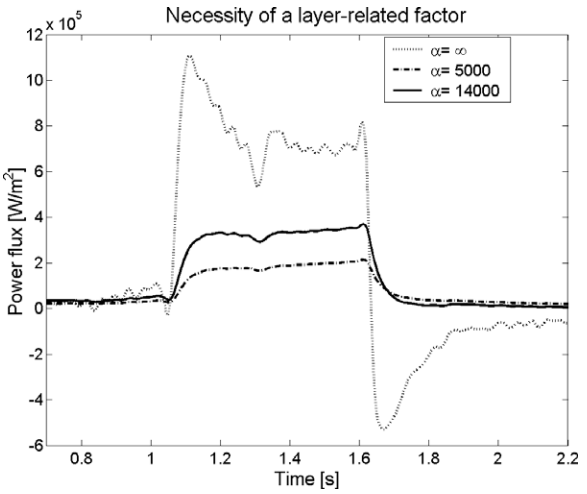

Fig. 5. Showing the effect of the layer assumption on the power fluxes calculated by THEODOR: no layers (in blue, $\alpha = \infty$) lead to unphysical artifacts at the beginning and end of the discharge, a too thick layer (dashed line, $\alpha = 5000\ \mathrm{W/m^2/K}$) results in too low a power flux (verified by tile thermometry), and the best estimate ($\alpha = 14000\ \mathrm{W/m^2/K}$) indicated by the solid line, from TCV shot #29979.

4.2.2.3. Tile misalignments. Section 4.2.1 has already raised the possibility that unmeasured tilt angles of the divertor floor tiles can lead to errors in the determination of γ. The TCV floor tiles are nominal perfectly horizontal (with radi used edges to reduce overheating there due to misalignment) but in practice, imperfections (toroidal non-uniformities) in the vacuum vessel mean that the ideal flat surface is never achieved. Matthews [19] used these imperfections in DIII-D to test the sin ϑ dependence in (3), but we do not yet have measurements of the tilt angle variation. For small attack angles, shadowing of the LP tile by its neighbour could mean that the probe $A_\perp$ and hence the j_{sat} is underestimated, leading to an overestimate of γ (which is actually observed for $\vartheta = 1°$, Fig. 2). To first order, if the LP tile were tilted w.r.t. the horizontal and shadowed by the adjacent tile, toroidal variations of the power along the tile might be expected to be observed. We have made a qualitative check of the misalignment influence by comparing the IR power across the LP tile surface, verifying that the radial power profile is toroidally similar within experimental scatter on both sides of the probe array (see Fig. 4). Whilst this seems to confirm that tile shadowing at low values of ϑ is not an issue, careful analysis shows that the power flux to the neighbouring tile is indeed ~25% higher than on the LP tile, even for higher values of ϑ. This can in fact clearly be seen from the 2D surface temperature image in Fig. 1 (for which $\vartheta = 1.8°$), showing that the neighbouring tile to the right of the probe tile is hotter. Being less than 0.1% at the tile location, toroidal field ripple as a possible explanation for the toroidal variations can be excluded. In-vessel measurements (which are planned) will be required to obtain the distribution of tilt angles across the divertor target area and thus determine if this can be responsible for the observed tile to tile power distribution.

4.3. Verification with thermocouple measurements and ANSYS simulations

The uncertainties discussed above can accumulate to values of 70%, leaving a rather wide margin for a robust comparison of the experimental transmission coefficients with theory. We have therefore attempted to cross-check the derived IR powers thermometrically, using a small array of thermocouples embedded in a tile neighbouring the LP tile and in the approximate region of the outer strike point (see Fig. 1). An accurate estimate of the total energy deposited into the tile from the single-point measurements supplied by the thermocouples is not straightforward. For the specific case of after-shot cooling, however, the time-scales of heat diffusion within the tile and heat transport away from the tile separate fairly well, with the latter being 1–2 orders of magnitude slower. We have verified this using 2D ANSYS simulations for our specific tiles (including a temperature dependent heat diffusion) with the experimentally measured heat loads as input. After only 5 s from the end of the applied heat pulse, the heat has distributed evenly in the tile (temperature differences of $<1\%$) such that the thermocouple reading is a good approximation for the temperature everywhere in the tile. After the initial redistribution of heat, our tile cools conductively (radiative cooling is negligible for the $\sim$30 °C tile temperature increase observed during the 1.5 s TCV pulse), showing an exponential time dependence. For the first 5 s, when the distribution is still very inhomogeneous, we have extrapolated the fitted cooling curve backwards, as is common practice for example on JET [20], to provide an estimate of the tile-averaged temperature. The stored energy is then simply an integral of the heat capacity of the tile between the maximal (as found by backward extrapolation) and final temperatures. Using this approach, we find good agreement between IR and thermocouple total deposited energies, with a maximum discrepancy of $\sim 15\%$ between the two diagnostics.

5. Conclusions

Using a combination of Langmuir probe arrays viewed by a 2D IR thermography system, sheath heat transmission factors have been measured for the first time in TCV. Radial profiles of γ have been obtained at the outer divertor of L-mode, single null lower diverted discharges encompassing variation in field line attack angle and plasma fuel species (D, He). The observed values of γ in the range 6 ± 2 for $\vartheta = 1$–$3°$, are consistent (but in general slightly lower), within error bars, with expected theory when neglecting particle reflection, secondary electron emission, surface recombination and assuming $T_i = T_e$.

Acknowledgement

This work was partially supported by the Swiss National Science Foundation.

References

[1] A. Herrmann et al., JNM 220–222 (1995) 543.
[2] D. Buchenauer et al., Rev. Sci. Instrum. 827 (1995).
[3] R.D. Monk et al., JNM 241–243 (1997) 396.
[4] N. Asakura et al., NF 35 (1995) 381.
[5] D. Storek, NF 41 (2001) 1.
[6] L. Costanzo et al., JNM 290–293 (2001) 840.
[7] P.C. Stangeby, The Plasma Boundary of Magnetic Fusion Devices, IoP Publishing, 2000.
[8] M. Wischmeier, PhD thesis TH3176, EPFL 2005.
[9] E.G. Wintucky, Solid Films 84 (1981) 161.
[10] R.A. Pitts, G.F. Matthews, JNM 176&177 (1990) 877.
[11] W. Eckstein, NF 1 (Suppl.) (1991) 17.
[12] E.W. Thomas, NF 1 (Suppl.) (1991) 79.
[13] G.F. Matthews et al., NF 31 (1991) 1383.
[14] S. Lisgo (this conference).
[15] R.A. Pitts et al., NF 39 (1999) 1433.
[16] R.A. Pitts et al., Nucl. Fusion 43 (2003) 1145.
[17] A. Herrmann et al., ECA 25A (2001) 2109.
[18] G.F. Matthews, PPCF 36 (1994) 1595.
[19] G.F. Matthews et al., GA Report. A20308.
[20] P. Andrew, UKAEA, private communication.